

Self-consistent many-body approach to the electroproduction of hypernuclei

P. Bydžovský^{a,*}, D. Denisova^{a,b}, D. Petrellis^a, D. Skoupil^a, P. Veselý^a,

G. De Gregorio^{c,d}, F. Knapp^b, and N. Lo Iudice^e

^a *Nuclear Physics Institute, ASCR, 25068 Řež/Prague, Czech Republic*

^b *Institute of Particle and Nuclear Physics, Faculty of Mathematics and Physics,*

Charles University, V Holešovičkách 2, 180 00 Prague, Czech Republic

^c *Dipartimento di Matematica e Fisica, Università degli Studi della*

Campania "Luigi Vanvitelli", viale Abramo Lincoln 5, I-81 100 Caserta, Italy

^d *Istituto Nazionale di Fisica Nucleare, Complesso Universitario di Monte S. Angelo, Via Cintia, I-80 126 Napoli, Italy*

^e *Dipartimento di Fisica, Università di Napoli Federico II, 80126 Napoli, Italy*

(Dated: September 1, 2023)

The electroproduction of selected p - and sd -shell hypernuclei was studied within a many-body approach using realistic interactions between the constituent baryons. The cross sections were computed in the distorted-wave impulse approximation using two elementary amplitudes for the electroproduction of the Λ hyperon. The structure of the hypernuclei was investigated within the framework of the self-consistent Λ -nucleon Tamm-Dancoff approach and its extension known as the Λ -nucleon equation of motion phonon method. Use was made of the NNLO_{sat} chiral potential plus the effective Nijmegen-F YN interaction. The method was first implemented on light nuclei for studying the available experimental data and establishing a relation to other approaches. After this proof test, it was adopted for predicting the electroproduction cross section of the hypernuclei $^{40}_{\Lambda}\text{K}$ and $^{48}_{\Lambda}\text{K}$ in view of the E12-15-008 experiment in preparation at JLab. On the ground of these predictions, appreciable effects on the spectra are expected to be induced by the YN interaction.

PACS numbers: 21.80.+a, 13.60.-r, 13.60.Le, 25.30.-c

I. INTRODUCTION

Hypernuclei represent an important bridge between particle and nuclear physics. Their study is of great relevance to both hadron physics and nuclear structure [1, 2].

Their spectra offer a unique tool for studying the effective hyperon-nucleon (YN) interaction, especially its spin-dependent component which is not clearly deduced from scattering experiments [3–5]. The replacement of a nucleon with the Λ hyperon also allows one to investigate deeply-bound states of Λ as the hyperon is not Pauli blocked inside the hypernucleus. It is especially important to investigate these deeply-bound states in heavy hypernuclei with a large neutron excess, e.g. in $^{208}_{\Lambda}\text{Tl}$ [6], as the interior of such heavy systems is a good proxy of nuclear matter. The comparison of the hypernuclear spectra with the experimental data contributes to clarification of the reaction mechanism and nuclear structure models and offers an additional test-ground for the nuclear forces.

Among the reactions used to produce hypernuclei [1, 3], the electroproduction is of particular interest since the electromagnetic interaction is well known and can be treated perturbatively. In the assumed kinematics, with large (≈ 1 GeV) photon and kaon momenta, the reaction can be satisfactorily described in the distorted-wave impulse approximation (DWIA) [7–9]. Moreover, since the energy resolution achieved in experiments with electron

beams is better than that in hadron induced reactions [3], it is possible to extract more precise information about the reaction and the details of the effective YN interaction.

In order to analyze the data unambiguously one needs a reliable theoretical model where inherent approximations are clearly specified as well as the input information (elementary amplitude, structure calculations, and kaon distortion). Such a need emerged from a recent investigation [8] where the importance of the Fermi motion and other kinematic effects on the electroproduction of hypernuclei, induced by two elementary amplitudes, was pointed out thereby suggesting some limits of the predictive power of the existing DWIA calculations.

The Fermi motion effects were also investigated by Mart *et al.* [10, 11] in the electromagnetic production of the hypertriton utilizing the two-component form of the elementary production amplitude in a general reference frame [12]. Using the KAON-MAID [13] model for the elementary amplitude, Mart and Ventel [11] found that the Fermi motion effects are essential for a correct description of the hypertriton electroproduction. These effects were found to be sizable in the longitudinal part of the cross section in agreement with our recent conclusions made for heavier hypernuclei [8]. Therefore, in this work we will use the optimum on-shell approximation discussed in Ref. [8] which partially includes the Fermi motion via the proton optimum momentum thereby allowing the use of the on-energy-shell elementary amplitude.

In previous papers [7–9], we have investigated the cross section for the electroproduction of p -shell hypernuclei within a phenomenological shell-model, whose nucleon-nucleon (NN) and effective YN interactions were fitted

*bydzovsky@ujf.cas.cz

to very precise data from γ -ray spectroscopy [5].

In the present work we will use the p - and sd -shell hypernuclear space and investigate, in addition to the light systems, the medium-mass hypernuclei ${}^{28}_{\Lambda}\text{Al}$, ${}^{40}_{\Lambda}\text{K}$, and ${}^{48}_{\Lambda}\text{K}$. The electroproduction of the latter two hypernuclei will be measured in the E12-15-008 experiment planned at JLab [14, 15].

The excitation spectra of p -shell and sd -shell Λ -hypernuclei were investigated within several shell-model approaches using different hypernuclear wave functions [16–20]. In Ref. [19], the full $(sd)^n$ -space and the Saclay-Lyon A (SLA) elementary amplitude in the frozen-proton approximation were adopted to investigate the photoproduction of the medium-mass hypernuclei ${}^{28}_{\Lambda}\text{Al}$ and ${}^{40}_{\Lambda}\text{K}$. In Ref. [21], a simple elementary-production amplitude and particle-hole shell model configurations were used for determining the energy-dependent cross sections of the electroproduction of ${}^{40}_{\Lambda}\text{K}$. Recently, the antisymmetrized molecular dynamics was adopted for investigating the structure of light Λ -hypernuclei and their spin dependence through the ΛN interaction [22, 23]. The shell-model was also utilized for predicting the cross section of the photoproduction of ${}^{12}_{\Lambda}\text{B}$ [24]. A fully covariant model was employed in description of the photoproduction of ${}^{16}_{\Lambda}\text{N}$ [25]. In this calculation the nucleon and hyperon bound states were obtained by solving the Dirac equation with a static nuclear mean-field potential. The same approach was also adopted for describing the hadron-induced reactions [26]. In Refs. [27, 28] the photoproduction of ${}^{16}_{\Lambda}\text{N}$ and ${}^{12}_{\Lambda}\text{B}$ was studied in the relativistic distorted wave impulse approximation. Here the single particle (s.p.) bound states were solutions of the time-independent Dirac equation using scalar and vector potentials [27].

The study presented here is carried out within a microscopic self-consistent many-body approach which involves complex nuclear excitations. A Hartree-Fock (HF) s.p. basis is generated for Λ and nucleons from the effective YN interaction plus the chiral NNLO_{sat} $NN + NNN$ potential [29]. The residual Hamiltonian is diagonalized in the particle-hole basis $\{|p-h\rangle\}$ so obtained. This mean field approach, known as Tamm-Dancoff for hypernuclei (TD $_{\Lambda}$), was adopted for p -shell hypernuclei in Ref. [30].

Here, we show how to go beyond the mean field theories and extend the TD $_{\Lambda}$ by coupling the Λ -nucleon $p-h$ states to more complex excitations of the nuclear core. Such a goal is reached within the equation of motion phonon method (EMPM) applied to hypernuclei.

The nuclear EMPM, in its upgraded version [31], adopts the equations of motion to generate an orthonormal basis of n -phonon ($n = 0, 1, 2, \dots$) states. Such a basis is then adopted to diagonalize the residual Hamiltonian. This amounts to coupling the TD $p-h$ configurations to $np-nh$ states. The method can use any Hamiltonian and does not rely on approximations except for the truncation of the multiphonon space. It has been used for investigating bulk and spectroscopic properties of light

as well as heavy nuclei [32–35].

The formulation of the method for hypernuclei, which we call EMPM $_{\Lambda}$, has two variants. One couples the Λ particle to an even-even nuclear core [36]. This version is suitable for describing hypernuclei such as ${}^5_{\Lambda}\text{He}$, ${}^{17}_{\Lambda}\text{O}$, and ${}^{41}_{\Lambda}\text{Ca}$. The other variant describes the hypernuclear states as Λ - N particle-hole excitations of an even core [37, 38] within the TD $_{\Lambda}$ framework. This version is suitable for describing hypernuclei like ${}^4_{\Lambda}\text{H}$, ${}^{16}_{\Lambda}\text{N}$, ${}^{40}_{\Lambda}\text{K}$, and ${}^{48}_{\Lambda}\text{K}$. It is worth pointing out that the calculation presented here is self-consistent and parameter free.

The paper is organized as follows: Sec. II briefly introduces the formalism developed in Ref. [8] and used here to compute the cross sections in the DWIA. Sec. III deals with the TD $_{\Lambda}$ and EMPM $_{\Lambda}$ methods describing the structure of the hypernuclei. Calculation details are discussed in Sec. IV. In Sec. V, we first present the excitation spectra of the p -shell hypernuclei ${}^{12}_{\Lambda}\text{B}$ and ${}^{16}_{\Lambda}\text{N}$ and compare them with the experimental data as well as with our advanced shell model results [7, 8]. We then discuss the sd -shell hypernuclei ${}^{28}_{\Lambda}\text{Al}$, ${}^{40}_{\Lambda}\text{K}$, and ${}^{48}_{\Lambda}\text{K}$ and give predictions for the planned JLab experiment E12-15-008. The conclusions drawn from our study are given in Sec. VI.

II. THE CROSS SECTION

The model for computing the cross section of the electroproduction of hypernuclei associated with a kaon in the final state

$$e + A \longrightarrow e' + H + K^+ \quad (1)$$

is described in Ref. [8].

The triple differential cross section in the nucleus-rest frame is

$$\frac{d^3\sigma}{dE'_e d\Omega'_e d\Omega_K} = \Gamma \frac{d\sigma}{d\Omega_K}, \quad (2)$$

where

$$\frac{d\sigma}{d\Omega_K} = \frac{d\sigma_{\text{T}}}{d\Omega_K} + \varepsilon_{\text{L}} \frac{d\sigma_{\text{L}}}{d\Omega_K} + \varepsilon \frac{d\sigma_{\text{TT}}}{d\Omega_K} + \sqrt{\varepsilon_{\text{L}}(\varepsilon + 1)} \frac{d\sigma_{\text{TL}}}{d\Omega_K}. \quad (3)$$

Here ε_{L} and ε are the longitudinal and transverse virtual-photon polarizations, respectively, and Γ is the virtual photon flux [8]. The separate cross sections are

$$\frac{d\sigma_{\text{T}}}{d\Omega_K} = \frac{\beta}{2[J_A]^2} \sum_{J_m} \frac{1}{[J]^2} (|A_{J_m}^{+1}|^2 + |A_{J_m}^{-1}|^2), \quad (4)$$

$$\frac{d\sigma_{\text{L}}}{d\Omega_K} = \frac{\beta}{[J_A]^2} \sum_{J_m} \frac{1}{[J]^2} |A_{J_m}^0|^2, \quad (5)$$

$$\frac{d\sigma_{\text{TT}}}{d\Omega_K} = \frac{\beta}{[J_A]^2} \sum_{J_m} \frac{1}{[J]^2} \text{Re}[A_{J_m}^{+1} A_{J_m}^{-1*}], \quad (6)$$

$$\frac{d\sigma_{\text{TL}}}{d\Omega_K} = \frac{\beta}{[J_A]^2} \sum_{Jm} \frac{1}{[J]^2} \text{Re}[A_{Jm}^{0*}(A_{Jm}^{+1} - A_{Jm}^{-1})], \quad (7)$$

where $[J] = \sqrt{2J+1}$ and β is the kinematical factor [8]. The transverse part (4) corresponds to the photoproduction cross section.

The reduced amplitudes A_{Jm}^μ have the form

$$A_{Jm}^\mu = \frac{1}{[J]} \sum_{rs} \mathcal{W}_{Jm}^\mu(rs) (\Psi_H || (b_r^\dagger \times a_s)^J || \Phi_A), \quad (8)$$

where

$$\mathcal{W}_{Jm}^\mu(rs) = \sum_{LS} \mathcal{H}_{l'j'l_j}^{LSJ} (\mathcal{R}_{(rs)}^L \times \mathcal{F}_\mu^{S\eta})^{Jm}. \quad (9)$$

Here, the label μ denotes the virtual photon helicity, S the spin transfer, and L the orbital momentum in the photon-kaon system. $\mathcal{H}_{l'j'l_j}^{LSJ}$ is a geometrical factor [8] which includes 3j and 9j symbols, $\mathcal{F}_\mu^{S\eta}$ the elementary production amplitude, and $\mathcal{R}_{(rs)}^{LM}$ the radial integral which includes the kaon distortion and the proton (s) and Λ (r) s.p. wave functions. Here the radial integrals are calculated using the HF s.p. wave functions under the assumptions described in Ref. [8] for the kaon distortion, consistently with the hypernuclear structure calculations.

A crucial role is played by nuclear structure through the one-body density matrix elements (OBDME) $(\Psi_H || (b_r^\dagger \times a_s)^J || \Phi_A)$. This quantity is computed within the framework of the TD_Λ approach and its multiphonon extension EMPM_Λ . To this purpose we use the $NN + NNN$ chiral potential NNLO_{sat} [29] plus the renormalized G-matrix Nijmegen-F ΛN interaction (NF YNG) [39] with various Fermi momenta k_F . Both approaches are described in the following section.

III. NUCLEAR STRUCTURE METHODS

A. Tamm-Dancoff approach for hypernuclei (TD_Λ)

Let us consider the angular momentum (J_λ) coupled basis states

$$|(p \times h^{-1})^\lambda\rangle = (b_p^\dagger \times a_h)^\lambda |0\rangle, \quad (10)$$

where b_p^\dagger creates the Λ particle p and a_h a nucleon hole h^{-1} out of the nuclear unperturbed HF ground state $|0\rangle$.

Such a basis is adopted to solve the eigenvalue equation

$$\begin{aligned} \langle (p \times h^{-1})^\lambda | H | \lambda \rangle &= \sum_{p'h'} \left([(\epsilon_p - \epsilon_h) - \omega_\lambda] \delta_{pp'} \delta_{hh'} \right. \\ &\left. + \langle (p \times h^{-1})^\lambda | V_{\Lambda N} | (p' \times h'^{-1})^\lambda \rangle \right) c_{p'h'}^\lambda, \end{aligned} \quad (11)$$

where $V_{\Lambda N}$ is the ΛN potential and

$$\omega_\lambda = E_\lambda - E_{\text{HF}}. \quad (12)$$

The eigenstates are

$$| \lambda \rangle = Q_\lambda^\dagger | 0 \rangle = \sum_{ph} c_{ph}^\lambda | (p \times h^{-1})^\lambda \rangle. \quad (13)$$

The above equation defines Q_λ^\dagger as an operator which creates TD_Λ hypernuclear phonons. The amplitudes c_{ph}^λ yield the TD_Λ OBDME

$$c_{ph}^\lambda = \frac{1}{[J_\lambda]} \langle \lambda || (b_p^\dagger \times a_h)^\lambda || 0 \rangle. \quad (14)$$

The TD formalism for the nucleonic excitations is exactly the same. We need to replace the ΛN potential $V_{\Lambda N}$ with the NN interaction V_{NN} and the Λ with a nucleon particle. We obtain

$$| \sigma \rangle = O_\sigma^\dagger | 0 \rangle = \sum_{ph} c_{ph}^\sigma | (p \times h^{-1})^\sigma \rangle. \quad (15)$$

B. Beyond TD_Λ : The EMPM_Λ

We now construct the basis of orthonormal n -phonon states $|\beta_n\rangle$ out of the redundant set

$$| \lambda \alpha_n \rangle = Q_\lambda^\dagger | \alpha_n \rangle, \quad (16)$$

where α_n is an n -phonon ($n = 1, 2, \dots$) state describing nuclear excitations and is composed of n nuclear TD phonons.

We first extract from the redundant set a basis of linearly independent (but not orthogonal) states $|\lambda \alpha_n\rangle$ through the Cholesky decomposition method. We then start with the equations of motion

$$\langle \alpha_n | [Q_\lambda, H] | \beta_n \rangle = (E_{\beta_n} - E_{\alpha_n}) \langle \lambda \alpha_n | \beta_n \rangle, \quad (17)$$

where Q_λ is the adjoint of the TD_Λ phonon creation operator.

After expanding the commutator and performing additional manipulations, we get the generalized eigenvalue equations

$$\sum_{jk} \left(\mathcal{H}_{ik}^{\beta_n} - E_{\beta_n} \delta_{ik} \right) \mathcal{D}_{kj}^{\beta_n} C_j^{\beta_n} = 0. \quad (18)$$

Here

$$\begin{aligned} \mathcal{H}_{ik}^{\beta_n} &= \mathcal{H}_{\lambda \alpha_n \lambda'' \alpha''_n}^{\beta_n} = \\ &= (E_\lambda + E_{\alpha_n}) \delta_{\lambda \lambda''} \delta_{\alpha_n \alpha''_n} + \mathcal{V}_{\lambda \alpha_n \lambda'' \alpha''_n}^{\beta_n}, \end{aligned} \quad (19)$$

where $\mathcal{V}_{\lambda \alpha_n \lambda'' \alpha''_n}^{\beta_n}$ defines the phonon-phonon interaction, and

$$\mathcal{D}_{ij}^{\beta_n} = \mathcal{D}_{\lambda \alpha_n \lambda' \alpha'_n}^{\beta_n} = \langle \lambda' \alpha'_n | \lambda \alpha_n \rangle \quad (20)$$

is the overlap or metric matrix which preserves the Pauli principle. The expressions for \mathcal{D} and \mathcal{V} can be found, for instance, in Ref. [31].

The n -phonon eigenstates so obtained have the form

$$|\beta_n\rangle = \sum_{\lambda\alpha_n} C_{\lambda\alpha_n}^{\beta_n} |\lambda\alpha_n\rangle. \quad (21)$$

The iteration of the procedure up to an arbitrary n produces a set of states which, added to the TD_Λ states $\{|\beta_0\rangle\} = \{|\lambda\rangle\}$, form an orthonormal basis $\{|\beta_n\rangle\}$ ($n = 0, 1, 2, 3, \dots$).

Such a basis is used for constructing and solving the eigenvalue problem in the full space

$$\sum_{\beta_n\beta_{n'}} \left((E_{\beta_n} - \mathcal{E}_\nu) \delta_{\beta_n\beta_{n'}} + \mathcal{V}_{\beta_n\beta_{n'}} \right) \mathcal{C}_{\beta_{n'}}^\nu = 0, \quad (22)$$

where $\mathcal{V}_{\beta_n\beta_{n'}} = 0$ for $n' = n$.

The solution yields for the hypernuclei the eigenvectors

$$|\Psi_\nu\rangle = \sum_{n,\beta_n} \mathcal{C}_{\beta_n}^\nu |\beta_n\rangle = \sum_{\beta_0} \mathcal{C}_{\beta_0}^\nu |\beta_0\rangle + \sum_{\beta_1} \mathcal{C}_{\beta_1}^\nu |\beta_1\rangle + \sum_{\beta_2} \mathcal{C}_{\beta_2}^\nu |\beta_2\rangle + \dots \quad (23)$$

The same method yields for the ground state of the target nuclei

$$|\Phi_0\rangle = \sum_{n,\alpha_n} \mathcal{R}_{\alpha_n}^0 |\alpha_n\rangle = \mathcal{R}_0^0 |0\rangle + \sum_{\alpha_2} \mathcal{R}_{\alpha_2}^0 |\alpha_2\rangle + \dots \quad (24)$$

The absence of the one-phonon components are to be noticed. It is an effect of the self-consistent HF basis adopted. The OBDME are given by

$$\langle \Psi_\nu || (b_r^\dagger \times a_s)^\lambda || \Phi_0 \rangle = \sum_{n,\alpha_n,\beta_n} \mathcal{C}_{\beta_n}^\nu \mathcal{R}_{\alpha_n}^0 \langle \beta_n || (b_s^\dagger \times a_r)^\lambda || \alpha_n \rangle. \quad (25)$$

We consider the restricted space spanned by $|\beta_0\rangle = |\lambda\rangle$ and $|\beta_1\rangle$. Thus the OBDME are simply

$$\langle \Psi_\nu || (b_r^\dagger \times a_s)^\lambda || 0 \rangle = \sum_{\lambda} \mathcal{C}_\lambda^\nu \langle \lambda || (b_p^\dagger \times a_h)^\lambda || 0 \rangle \delta_{rp} \delta_{sh}. \quad (26)$$

It is important to notice that $\langle \beta_1 || (b_p^\dagger \times a_h)^\lambda || 0 \rangle = 0$. In order to get an additional contribution and, consequently, additional peaks in the cross section, we should enlarge the space so as to include the two-phonon basis states $|\alpha_2\rangle$ for the parent nuclei and/or hypernuclei. We would get contributions from

$$\langle \beta_1 || (b_r^\dagger \times a_s)^\lambda || \alpha_2 \rangle \propto \langle \lambda' || (b_p^\dagger \times a_{p'})^\lambda || \sigma \rangle \delta_{rp} \delta_{sp'} \quad (27)$$

and

$$\langle \beta_2 || (b_r^\dagger \times a_s)^\lambda || \alpha_2 \rangle \propto \langle \beta_0 = \lambda || (b_p^\dagger \times a_h)^\lambda || 0 \rangle. \quad (28)$$

IV. CALCULATION DETAILS

The Hamiltonian has the structure

$$H = T_{\text{intr}} + V = T_N + T_\Lambda - T_{\text{c.m.}} + V_{\text{sat}} + V_{\Lambda N}. \quad (29)$$

The intrinsic kinetic term T_{intr} is obtained by subtracting the center of mass term $T_{\text{c.m.}}$ from the kinetic terms of nucleons (T_N) and Λ (T_Λ), V_{sat} is the $NNLO_{\text{sat}}$ potential [29] which includes the NN and NNN interactions. The NNN component is fully taken into account in generating the HF basis, while it is truncated at the normal order two-body level in TD (TD_Λ) and the EMPM ($EMPM_\Lambda$). The residual NNN interaction does not enter into the TD (TD_Λ), which is therefore unaffected by the truncation.

The G-matrix derived from the Nijmegen-F interaction is parametrized as a sum of Gaussian-like terms [39]

$$V_{\Lambda N} = \sum_{i=1}^3 (a_i + b_i k_F + c_i k_F^2) \exp(-r^2/\beta_i^2) \quad (30)$$

and is used for various values of the Fermi momentum k_F . The a_i , b_i and c_i coefficients are given in [39].

Using the above potentials we have generated a HF basis for Λ as well as for the nucleons from a harmonic oscillator (HO) space sufficiently large in order to reach convergence with respect to the HO frequency. It is sufficient to use a HO basis with a number of major shells up to $N_{\text{max}} = 10$ for p -shell hypernuclei and $N_{\text{max}} = 12$ for sd -shell hypernuclei. The $EMPM_\Lambda$ is numerically more costly. Therefore, in $^{12}_\Lambda\text{B}$ and $^{16}_\Lambda\text{N}$ we restricted our space to $N_{\text{max}} = 8$ for the proton and neutron levels, while for Λ we took into account levels up to the sd -shell. In $^{28}_\Lambda\text{Al}$, $^{40}_\Lambda\text{K}$, and $^{48}_\Lambda\text{K}$, the $EMPM_\Lambda$ calculation is unreachable even for $N_{\text{max}} = 8$. Thus, we have generated the HF basis for $N_{\text{max}} = 12$ in order to obtain fully convergence for the nucleon s.p. states and then used a subset of such a basis corresponding to a HO space up to $N_{\text{max}} = 4$. The space for Λ is up to the sd -shell.

V. RESULTS

The cross sections were calculated in various kinematics using the elementary amplitudes BS3 [40] and SLA [41] in the optimum on-shell approximation [8]. We also considered the frozen-proton approximation in order to relate our findings to the results by Motoba *et al.* [19]. The kaon distortion was treated in the same manner as in our previous calculations [8]. Therefore, the differences with respect to the previous results are to be ascribed to the different methods adopted here to compute the transition densities OBDME and to the different forms of the YN interaction. The peaks were smoothed through Gaussians with a uniform width deduced from the experimental data or consistent with the width anticipated in planned experiments. The experimental background was not taken into account.

A. The $^{12}_{\Lambda}\text{B}$ hypernucleus

We used the NF YNG interaction with $k_F = 1.1 \text{ fm}^{-1}$ to compute the binding energy of Λ . This was extracted through the approximate formula

$$-B_{\Lambda} \simeq \mathcal{E}_{\text{g.s.}} + \epsilon_F^{\text{p}}, \quad (31)$$

where $\mathcal{E}_{\text{g.s.}}$ is the lowest TD_{Λ} (Eq. 12) or EMPM_{Λ} (Eq. 22) eigenvalue and ϵ_F^{p} is the energy of the last occupied proton orbit. We get $B_{\Lambda}^{(\text{TD})} = 10.37 \text{ MeV}$, smaller than the empirical binding energy $B^{(\text{exp})} = 11.37 \pm 0.06 \text{ MeV}$ [1, 7]. The EMPM_{Λ} value is larger instead ($B_{\Lambda}^{(\text{EM})} = 12.88 \text{ MeV}$).

In Fig. 1, the TD_{Λ} and EMPM_{Λ} energy distributions of the cross section are compared with the data produced by the E94-107 experiment [7] and analyzed within a shell model approach [7]. Such a calculation used a Woods-Saxon s.p. basis and an effective YN interaction fitted to the γ -ray spectroscopic data of the p -shell hypernuclei [5]. In Ref. [8], we analyzed the same data. To this purpose, we took the shell model OBDME from Ref. [7], but replaced the frozen-proton approximation adopted there with the optimum on-shell approximation. Such a replacement, complemented with other minor changes, has improved the agreement with the experimental data. In fact, both magnitudes and energy distribution of the transition strengths are well reproduced.

The TD_{Λ} and EMPM_{Λ} calculations were performed using a HF basis and they are parameter free except for the Fermi momentum k_F . This parameter was fixed so as to reproduce the empirical energy gap between the $(0p_{3/2})_{\Lambda}$ and $(0s_{1/2})_{\Lambda}$ states and resulted to be $k_F = 1.1 \text{ fm}^{-1}$. TD_{Λ} reproduces the two main peaks. Though slightly too high, they fall at the correct energies. The low and high energy peaks correspond to the $(0s_{1/2})_{\Lambda} - (0p_{3/2})_N^{-1}$ and $(0p_{3/2})_{\Lambda} - (0p_{3/2})_N^{-1}$ excitations. TD_{Λ} misses the observed strength in between. The coupling to the nuclear core TD phonons, within the EMPM_{Λ} , induces a damping of the two main peaks consistently with the data, but also a slight downward energy shift of the high energy peak. It produces also several transitions comparable in number with those observed experimentally. However, they are generally too weak and not always at the correct energies. It seems therefore necessary to enlarge the multiphonon space so as to include the two-phonon (2p-2h) configurations. As illustrated in Eqs. (27) and (28) this additional basis is expected to enhance the fragmentation of the cross section as well as the strengths of the existing intermediate transitions.

B. The $^{16}_{\Lambda}\text{N}$ hypernucleus

As for $^{12}_{\Lambda}\text{B}$, we used the NF YNG interaction with $k_F = 1.1 \text{ fm}^{-1}$. The TD_{Λ} binding energy is $B_{\Lambda}^{(\text{TD})} = 12.93 \text{ MeV}$, smaller than the empirical value $B^{(\text{exp})} = 13.76 \pm$

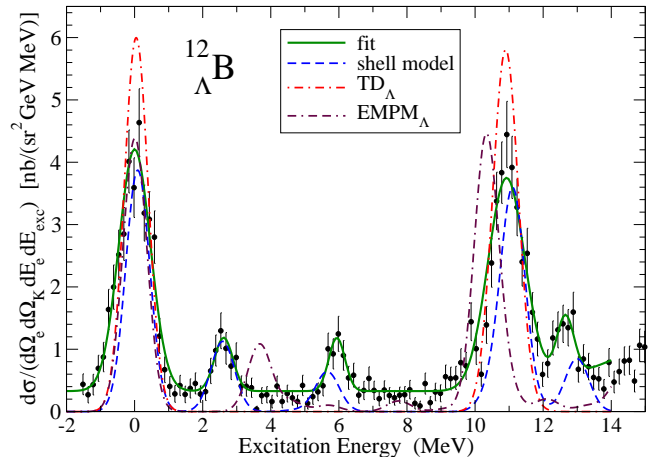


FIG. 1: The TD_{Λ} (dash-dot line), and EMPM_{Λ} (double-dash-dot line) spectra of $^{12}_{\Lambda}\text{B}$ are compared with the data [7] and an empirical shell-model calculation [7]. The calculations were performed using the BS3 elementary amplitude. The solid line is the fit to the data. The FWHM used in the calculation is 820 keV.

0.16 MeV [42]. The EMPM_{Λ} yields $B_{\Lambda}^{(\text{EM})} = 17.19 \text{ MeV}$, which is too large. It is necessary to explore if and how such a large discrepancy can be reduced. One may try to exploit the sensitivity to the Fermi momentum of the $V_{\Lambda N}$ potential.

We computed the cross section by the same shell model approach adopted for $^{12}_{\Lambda}\text{B}$. As shown in Fig. 2, the calculation tends to overestimate the magnitude of the peaks, just as in previous investigations [7, 8], suggesting the need of enlarging the shell-model space [7].

Unlike the case of $^{12}_{\Lambda}\text{B}$, the cross section obtained within TD_{Λ} , has the same peak composition of the experimental quantity (Fig. 2). The first and third peaks fall at the correct energies. They correspond to the $(0s_{1/2})_{\Lambda} - (0p_{1/2})_N^{-1}$ and $(0p_{3/2})_{\Lambda} - (0p_{1/2})_N^{-1}$ excitations, respectively. We observe, instead, an upward shift of the second and fourth peaks corresponding to the $(0s_{1/2})_{\Lambda} - (0p_{3/2})_N^{-1}$ and $(0p_{3/2})_{\Lambda} - (0p_{3/2})_N^{-1}$ configuration, an indication of a possible too large spin-orbit splitting. We could bring them to the experimental excitation energies if we multiply by a factor 1.2 the strength of the NNN component of the NNLO_{sat} potential, while keeping the same k_F in the YN potential.

The EMPM_{Λ} cross section keeps roughly the peak structure obtained in TD_{Λ} . However, it is rigidly shifted upward in energy by 1.83 MeV. Such a shift finds the following explanation. The lowest peak is generated by populating the excited 1_1^- state rather than the 0_1^- ground state which is shifted down in energy and carries a negligible strength. In TD_{Λ} , instead, these two states are almost degenerate, consistently with experimental γ -ray spectroscopy measurements of the mirror hypernucleus

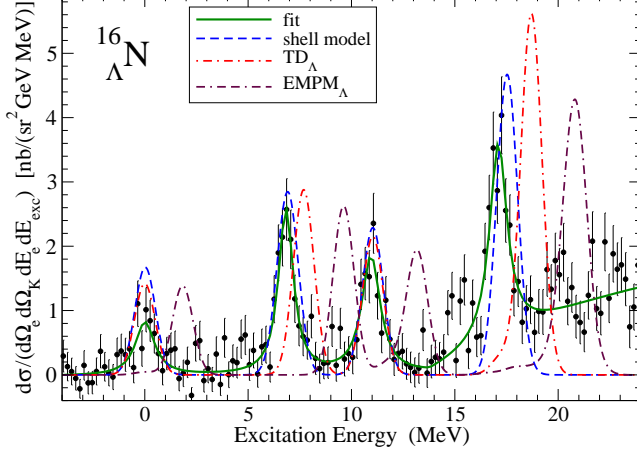


FIG. 2: The experimental spectrum of $^{16}_{\Lambda}\text{N}$ and its fit, taken from Ref. [7] are compared with the theoretical cross sections obtained within shell-model, TD_{Λ} , and EMPM_{Λ} using the BS3 elementary amplitude. The theoretical lines do not account for the background but the fit includes the background. The FWHM used here is 1177 keV.

$^{16}_{\Lambda}\text{O}$ [43]. It would be necessary to enlarge the multiphonon space in order to hopefully clarify the reason of such a deficiency.

C. The $^{28}_{\Lambda}\text{Al}$ hypernucleus

In the absence of experimental data, we estimated the Fermi momentum k_F entering the NF YNG potential in the Thomas-Fermi approximation. We have

$$k_F = \left(\frac{3\pi^2}{2} \langle \rho \rangle \right)^{1/3}, \quad (32)$$

where the average density $\langle \rho \rangle$ is calculated in the average density approximation (ADA)

$$\langle \rho \rangle = \int d^3r \rho_N(\vec{r}) \rho_{\Lambda}(\vec{r}). \quad (33)$$

Here $\rho_N(\vec{r})$ ($\rho_{\Lambda}(\vec{r})$) is the nucleon (Λ) density. For $^{28}_{\Lambda}\text{Al}$ we obtain $k_F = 1.24 \text{ fm}^{-1}$.

By using this value we obtain for the binding energy of Λ in its lowest s -orbit $B_{\Lambda}^{(\text{TD})} = 15.58 \text{ MeV}$ in TD_{Λ} and $B_{\Lambda}^{(\text{EM})} = 16.62 \text{ MeV}$ in EMPM_{Λ} , both close to the empirical value for $^{28}_{\Lambda}\text{Si}$ $B_{\Lambda}^{(\text{exp})} = 17.2 \text{ MeV}$ [1, 44].

Since the Thomas-Fermi approximation (32) provides just an estimate of k_F we investigate how sensitive are the cross sections to the Fermi momentum. The TD_{Λ} cross sections computed using three k_F values are plotted in Fig. 3 and compared with the photoproduction cross section computed within a phenomenological shell

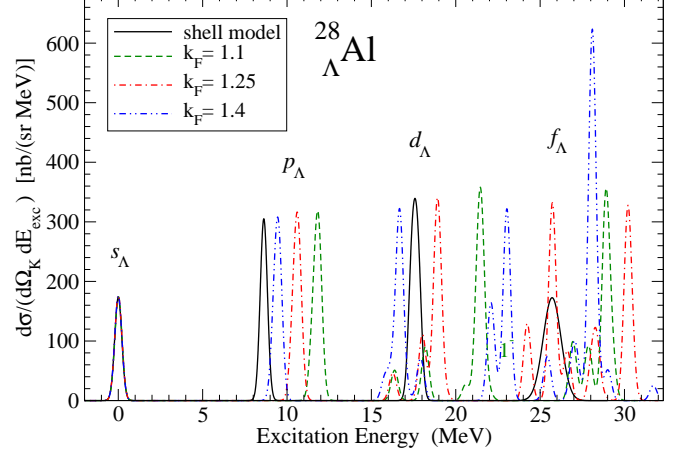


FIG. 3: The TD_{Λ} electroproduction cross section of $^{28}_{\Lambda}\text{Al}$, computed for three values of the Fermi momentum k_F [fm^{-1}] entering the NF YNG potential, is compared with the photoproduction cross section obtained within a phenomenological shell model by Motoba *et al* [19]. The peaks are drawn using the FWHM = 500 keV. The labels s , p , d , and f denote the Λ orbital quantum numbers of the ($p_{\Lambda} - \hbar^{-1}$) configurations generating the corresponding peaks. The differential cross section $d\sigma$ is given in nb/sr (Eq. (3)), while for $^{12}_{\Lambda}\text{B}$ and $^{16}_{\Lambda}\text{N}$ we plotted the triple-differential cross section in nb/(sr² GeV).

model approach by Motoba *et al* [19] using the universal sd -shell interaction (USD) [45] in the full $[s^4 p^{12} (sd)_{pn}^{12}]$ model space. Both calculations made use of the Saclay-Lyon A (SLA) elementary amplitude in the frozen-proton approximation. Note that the kinematics was $E_{\gamma} = 1.3 \text{ GeV}$ and $\theta_K = 3^{\circ}$ in the photoproduction and $E_i = 1.8 \text{ GeV}$, $E_f = 0.5 \text{ GeV}$, $\theta_e = 5.4^{\circ}$, $\theta_{Ke} = 5.1^{\circ}$, and $\Phi_K = 180^{\circ}$ in the electroproduction. Since the photon virtuality given by $Q^2 = -q_{\gamma}^2 = 0.008 \text{ (GeV/c)}^2$ is very small, the two approaches can be regarded as almost equivalent.

The cross section generated by the ground state doublet is practically the same in both approaches. Note the extreme sensitivity of the energy distribution of the peaks to k_F is to be noticed. The spectrum tends to be more and more compact as k_F increases. However, whatever k_F value is adopted, only a qualitative partial consistency between the shell-model and TD_{Λ} results can be achieved.

The very high peak at 28.1 MeV which exceeds 300 nb/sr is obtained for $k_F = 1.4 \text{ fm}^{-1}$ and originates from the envelope of many closely packed transitions. The main contribution comes from the states 4^+ , 7^+ , and 5^+ at $E = 27.979 \text{ MeV}$, $E = 28.122 \text{ MeV}$, and $E = 28.142 \text{ MeV}$, respectively. These states are mostly populated through the transition from the $0d_{5/2}$ proton to the final $1d_{3/2}$ (4^+), $1d_{5/2}$ (7^+), and $0g_{9/2}$ (5^+) Λ orbits. The peak at

≈ 23 MeV, whose magnitude is about half, is produced by the transitions to the 6^- and 5^- states, obtained by creating a $(0f_{7/2})_\Lambda$ and $(0f_{5/2})_\Lambda$ at the expense of a $0d_{5/2}$ proton.

D. The $^{40}_\Lambda\text{K}$ hypernucleus

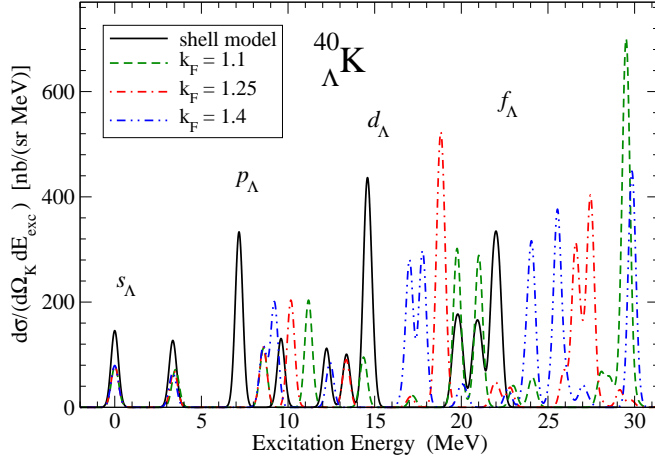


FIG. 4: The same as in Fig. 3 but for $^{40}_\Lambda\text{K}$.

In $^{40}_\Lambda\text{K}$, not only the position, as in $^{28}_\Lambda\text{Al}$, but also the height of the TD_Λ peaks changes considerably with k_F (Fig. 4). Also for this system, the agreement with the shell model spectrum is only partial for any k_F .

In this stage, it may be worthwhile to make some predictions for the spectrum of $^{40}_\Lambda\text{K}$ in view of the planned JLab E12-15-008 experiment [14]. For this purpose, we used the following kinematics of the experiment [15]: $E_i = 2.24$ GeV, $E_f = 0.74$ GeV, $\theta_e = 8^\circ$, $\theta_{Ke} = 11^\circ$, and $\Phi_K = 180^\circ$, which generates kinematics of the virtual photon $E_\gamma = 1.5$ GeV, $\theta_{K\gamma} = 7.1^\circ$, $Q^2 = 0.032$ (GeV/c) 2 , and $\epsilon = 0.591$. We used the FWHM = 800 keV which we deem to be suitable for the planned experiment.

The TD_Λ and EMPM_Λ strength distributions were computed using $k_F = 1.25$ fm $^{-1}$ and the BS3 amplitude in the optimum on-shell approximation. The two spectra, calculated in kinematics of the E12-15-008 experiment, are very close (Fig. 5). The number of peaks is comparable in both cases. One may only notice the damping effect induced by the coupling of TD_Λ to the nuclear core excitations, described by TD phonons, which reduces systematically the heights of EMPM_Λ peaks. Such a coupling induces also a slight upward displacement of the peaks which increases with energy. For instance, the first excited state 2^+ , nearly degenerate with the ground state 1^+ in TD_Λ , is shifted up to 0.269 MeV in EMPM_Λ . The strongly populated EMPM_Λ states 1^+ and 3^+ are ≈ 0.6

MeV above the corresponding TD_Λ states at 3.42 and 8.57 MeV, respectively.

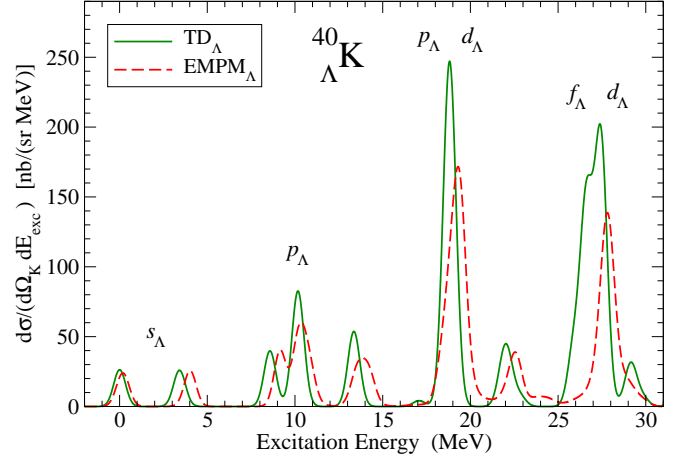


FIG. 5: The spectrum of $^{40}_\Lambda\text{K}$ calculated within the TD_Λ and EMPM_Λ approaches with $k_F = 1.25$ fm $^{-1}$ in kinematics of the E12-15-008 experiment.

The coupling to the nuclear core phonons induces an increment of 1.35 MeV to the binding energy of Λ . Using Eq. (31), we get for $k_F = 1.25$ fm $^{-1}$ $B_\Lambda^{(\text{TD})} = 18.62$ MeV in TD_Λ and $B_\Lambda^{(\text{EM})} = 19.97$ MeV in the EMPM_Λ where the former agrees very well with the value $B_\Lambda = 18.70$ MeV calculated from the Λ -nucleus optical potential [44]. The enhanced value of $B_\Lambda^{(\text{EM})}$ may indicate a need for elaborating the EMPM_Λ method as we have mentioned it in the case of the ^{12}C and ^{16}O targets but this value is not so bad if we compare it with another empirical value ≈ 19.7 MeV obtained from a Woods-Saxon potential in Fig. 11 of Ref. [1].

Since the target ^{40}Ca is a closed-shell nucleus, we expect reliable predictions from the TD_Λ (particle-hole) approach as was the case of the reactions using ^{16}O as target (Fig. 2). As shown in Fig. 6, the TD_Λ spectrum is affected by the elementary amplitude adopted. The BS3 amplitude yields significantly larger cross sections with respect to SLA (see also Table I). However, the above differences are smaller than the differences between the photoproduction, given roughly by ds_T , and the electroproduction cross sections obtained by using the BS3 amplitude. Although the photon virtuality Q^2 is quite small here, contributions from the longitudinal response functions to the full cross section are important.

The hypernucleus states populated in kinematics of E12-15-008 with cross sections larger than 5 nb/sr are displayed in Table I. The proton and Λ s.p. states with the dominant transition given by OBDME in Eq. (8) are also shown. The first five states are deeply bound with the Λ predominantly in the $0s_{1/2}$ orbit. Consistently with the results, in Fig. 4 of Ref. [21] one may notice the

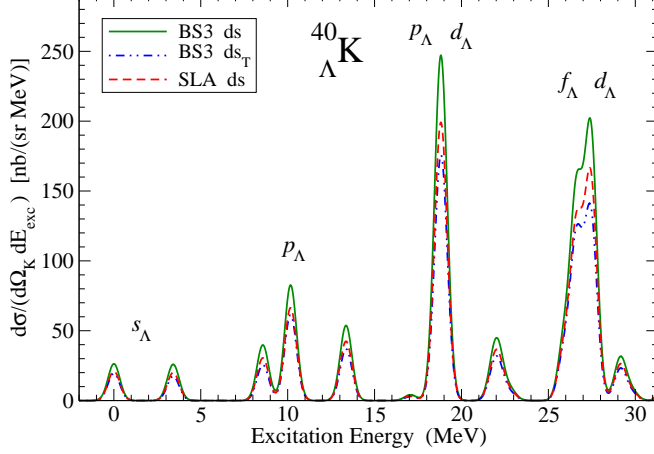


FIG. 6: Electroproduction (ds) cross sections of $^{40}_{\Lambda}\text{K}$ computed within TD_{Λ} using the BS3 and SLA elementary amplitudes in the optimum on-shell approximation. The photo-production (ds_T), computed with the BS3 amplitude, is also shown. The used FWHM is 800 keV.

deeply-bound states 3^+ and 2^+ with the Λ in the $0s_{1/2}$ orbit and the strongly populated substitutional states 3^+ at $E_x = 18.917$ MeV and the 1^+ at $E_x = 21.862$ MeV, produced upon replacing a proton with the Λ in the same orbit. Similar results were obtained within the shell model [19].

E. The $^{48}_{\Lambda}\text{K}$ hypernucleus

In $^{48}_{\Lambda}\text{K}$, the coupling of TD_{Λ} to the nuclear core excitations within the EMPM_{Λ} has the effect of incrementing the binding of Λ by 1.51 MeV, to be added to the binding obtained with TD_{Λ} . For $k_F = 1.25 \text{ fm}^{-1}$, $B_{\Lambda}^{(\text{TD})} = 20.01$ MeV, which is fairly close to the value $B_{\Lambda} = 19.78$ MeV obtained in the calculations with the Λ -nucleus optical potential [44].

This coupling induces also a damping and an additional fragmentation of the cross section which modifies the shapes of the peaks in the spectrum similarly as for the $^{40}_{\Lambda}\text{K}$ in Fig. 5. Finally, it should be pointed out that the magnitude of the peaks is also affected by the elementary amplitude [7, 8] (Fig. 7) as well as by kinematical and other effects [8, 9]. The shape of the spectrum differs from the one predicted for $^{40}_{\Lambda}\text{K}$ (Fig. 6) and the cross sections are in general smaller.

In Table II, we show the electroproduction cross sections of $^{48}_{\Lambda}\text{K}$. The ground state 0^+ cross section is negligible whereas the first excited state 1^+ is quite strongly populated. This can be easily explained. Since the cross section is determined mainly by the s.p. transition $1s_{1/2} \rightarrow 0s_{1/2}^{\Lambda}$, only the $L = 0$ in Eq. (8) contributes so that the production amplitude is determined by the

E_x (MeV)	J^P	s.p. states		cross sections	
		p	Λ	SLA	BS3
0.000	1^+	$0d_{3/2}$	$0s_{1/2}$	4.47	7.55
0.004	2^+	$0d_{3/2}$	$0s_{1/2}$	13.43	14.84
3.417	1^+	$1s_{1/2}$	$0s_{1/2}$	17.02	21.77
8.570	3^+	$0d_{5/2}$	$0s_{1/2}$	17.34	24.53
8.578	2^+	$0d_{5/2}$	$0s_{1/2}$	8.63	9.36
10.161	2^-	$0d_{3/2}$	$0p_{1/2}, 0p_{3/2}$	18.54	28.12
10.164	3^-	$0d_{3/2}$	$0p_{3/2}$	36.49	40.42
13.351	1^-	$1s_{1/2}$	$0p_{1/2}, 0p_{3/2}$	17.56	17.82
13.361	2^-	$1s_{1/2}$	$0p_{3/2}$	17.56	23.69
18.511	2^+	$0d_{3/2}$	$1s_{1/2}$	6.07	6.41
18.712	3^-	$0d_{5/2}$	$0p_{1/2}, 0p_{3/2}$	29.32	30.92
18.740	4^-	$0d_{5/2}$	$0p_{3/2}$	50.10	69.25
18.917	3^+	$0d_{3/2}$	$0d_{3/2}$	30.20	43.14
18.924	4^+	$0d_{3/2}$	$0d_{5/2}$	49.51	54.19
18.970	2^-	$0d_{5/2}$	$0p_{1/2}, 0p_{3/2}$	4.78	6.13
21.862	1^+	$1s_{1/2}$	$1s_{1/2}$	14.87	18.07
22.128	2^+	$1s_{1/2}$	$0d_{3/2}$	6.64	6.54
22.138	3^+	$1s_{1/2}$	$0d_{5/2}$	6.95	9.36
25.887	2^-	$0d_{3/2}$	$1p_{1/2}$	10.12	14.67
25.905	3^-	$0d_{3/2}$	$1p_{3/2}$	18.31	19.35
26.577	4^-	$0d_{3/2}$	$0f_{5/2}$	34.78	48.07
26.586	5^-	$0d_{3/2}$	$0f_{7/2}$	52.12	56.21
26.947	2^+	$0p_{1/2}$	$0p_{3/2}$	9.06	9.78
27.031	3^+	$0d_{5/2}$	$1s_{1/2}$	9.05	11.82
27.345	4^+	$0d_{5/2}$	$0d_{5/2}$	6.93	7.39
27.463	4^+	$0d_{5/2}$	$0d_{3/2}$	43.34	44.47
27.475	5^+	$0d_{5/2}$	$0d_{5/2}$	67.84	91.17
29.139	1^-	$1s_{1/2}$	$1p_{1/2}$	10.82	10.60
29.148	2^-	$1s_{1/2}$	$1p_{3/2}$	10.65	13.44

TABLE I: The cross sections predicted in electroproduction of $^{40}_{\Lambda}\text{K}$ for selected hypernucleus states given by E_x and J^P . The calculations were done in the TD_{Λ} formalism with the NF YNG interaction and $k_F = 1.25 \text{ fm}^{-1}$ for two elementary amplitudes SLA and BS3 in the optimum on-shell approximation. The s.p. states of the proton (p) and Λ , denoted by r and s in Eq. (8), for the dominant OBDME are shown. The differential cross section is in nb/sr.

spin $J = S$. In the considered kinematics the $S = 1$ elementary amplitude (Eq. (9)) is more than one order of magnitude larger than the $S = 0$ one and, consequently, the cross sections are larger by two orders of magnitude.

The order of the deepest states 1^+ and 2^+ in Table II, dominated by the $(0s_{1/2})_{\Lambda} - (1s_{1/2})_p$ and $(0s_{1/2})_{\Lambda} - (0d_{3/2})_p$ configurations, respectively, is reversed with respect to Table I. This effect is caused by different relative energy gap of the proton $0d_{3/2}$ and $1s_{1/2}$ orbitals. In ^{40}Ca ($\epsilon_p(0d_{3/2}) - \epsilon_p(1s_{1/2})$) = 3.22 MeV while in ^{48}Ca ($\epsilon_p(0d_{3/2}) - \epsilon_p(1s_{1/2})$) = -1.44 MeV. The orbits $0d_{3/2}$ and $1s_{1/2}$ switch their positions as a result of the proton-neutron interaction in ^{48}Ca with the neutron excess.

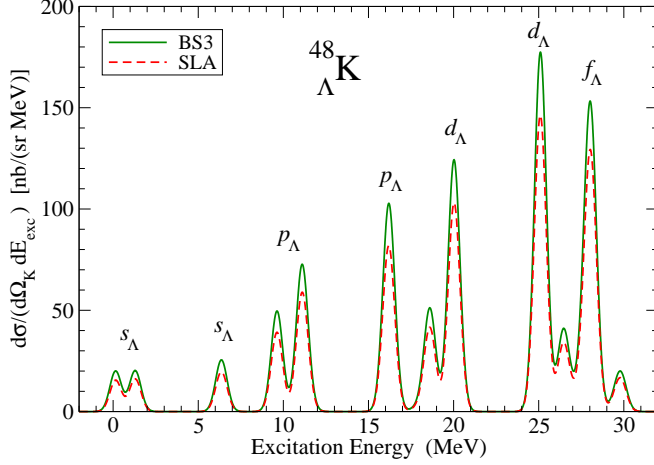


FIG. 7: TD_Λ $^{48}_\Lambda\text{K}$ spectrum computed with the BS3 and SLA elementary amplitudes in the optimum on-shell approximation and kinematics of the E12-15-008 experiment.

As for $^{40}_\Lambda\text{K}$, appreciable differences between the SLA and BS3 cross sections can be observed for some peaks (Fig. 7). However, these differences are smaller than the uncertainties caused by neglecting the contributions from the longitudinal mode of the virtual photon. Also in $^{48}_\Lambda\text{K}$, the high energy substitutional states 1^+ , 3^+ , and 5^+ are strongly populated and the 1^+ , 2^+ , and 3^+ states with Λ in the $0s_{1/2}$ orbit are deeply bound (Table II).

VI. CONCLUSIONS

We expanded our previous calculations for the electroproduction of p -shell hypernuclei to the production of medium-mass (sd -shell) hypernuclei and performed a preliminary analysis of the results. To this end we adopted new formalisms, TD_Λ and its extension EMPM_Λ , in order to study the effect of the hypernuclear structure, determined by the OBDME, on the cross sections computed in DWIA.

Using the effective Nijmegen YN interaction and two amplitudes for the elementary production in the optimum on-shell and frozen-proton approximations, we analyzed the dependence of the energy spectra on the interaction for different values of the Fermi momentum k_F and estimated the uncertainties from various inputs (elementary amplitudes, Fermi motion).

The results for the light hypernuclei $^{12}_\Lambda\text{B}$ and $^{16}_\Lambda\text{N}$ were compared with the experimental data as well as with our previous calculations using a phenomenological shell-model. A reasonable agreement was obtained for $^{16}_\Lambda\text{N}$ whereas our new results for $^{12}_\Lambda\text{B}$ agree only for the two main peaks of the spectrum. In the medium-mass hypernuclei $^{28}_\Lambda\text{Al}$ and $^{40}_\Lambda\text{K}$, the cross sections were compared with older shell-model results. We give also predictions

E_x (MeV)	J^P	s.p. states		cross sections	
		p	Λ	SLA	BS3
0.148	1^+	$1s_{1/2}$	$0s_{1/2}$	13.14	16.80
1.294	1^+	$0d_{3/2}$	$0s_{1/2}$	3.41	5.67
1.297	2^+	$0d_{3/2}$	$0s_{1/2}$	10.30	11.52
6.359	3^+	$0d_{5/2}$	$0s_{1/2}$	11.14	15.61
6.364	2^+	$0d_{5/2}$	$0s_{1/2}$	5.56	6.10
9.578	1^-	$1s_{1/2}$	$0p_{1/2}$	14.43	14.69
9.657	2^-	$1s_{1/2}$	$0p_{3/2}$	17.05	23.06
11.068	2^-	$0d_{3/2}$	$0p_{1/2}, 0p_{3/2}$	13.19	20.63
11.117	3^-	$0d_{3/2}$	$0p_{3/2}$	31.59	35.02
15.975	3^-	$0d_{5/2}$	$0p_{1/2}, 0p_{3/2}$	6.38	6.71
16.140	3^-	$0d_{5/2}$	$0p_{1/2}, 0p_{3/2}$	19.37	20.67
16.217	4^-	$0d_{5/2}$	$0p_{3/2}$	39.09	53.65
16.417	2^-	$0d_{5/2}$	$0p_{1/2}, 0p_{3/2}$	5.32	6.65
18.485	2^+	$1s_{1/2}$	$0d_{3/2}$	7.01	6.95
18.603	3^+	$1s_{1/2}$	$0d_{5/2}$	8.45	11.43
18.671	1^+	$1s_{1/2}$	$1s_{1/2}$	15.58	18.92
19.941	3^+	$0d_{3/2}$	$0d_{3/2}$	22.13	30.54
20.006	3^+	$0d_{3/2}$	$0d_{5/2}$	7.42	10.49
20.067	4^+	$0d_{3/2}$	$0d_{5/2}$	46.85	51.12
24.911	3^+	$0d_{5/2}$	$0d_{3/2}$	6.64	6.93
24.980	4^+	$0d_{5/2}$	$0d_{3/2}, 0d_{5/2}$	28.51	28.96
25.065	4^+	$0d_{5/2}$	$0d_{3/2}, 0d_{5/2}$	17.88	18.90
25.155	5^+	$0d_{5/2}$	$0d_{5/2}$	62.02	82.93
25.248	3^+	$0d_{5/2}$	$0d_{5/2}, 1s_{1/2}$	6.54	7.85
26.430	1^-	$1s_{1/2}$	$1p_{1/2}$	10.95	10.73
26.441	2^-	$1s_{1/2}$	$1p_{3/2}$	12.14	15.29
27.434	2^+	$0p_{1/2}$	$0p_{3/2}$	5.09	5.60
27.813	2^-	$0d_{3/2}$	$1p_{1/2}$	4.20	5.68
27.820	2^-	$0d_{3/2}$	$1p_{3/2}$	5.06	7.27
27.847	3^-	$0d_{3/2}$	$1p_{3/2}$	15.71	16.62
28.013	4^-	$0d_{3/2}$	$0f_{5/2}$	28.78	40.07
28.077	4^-	$0d_{3/2}$	$0f_{7/2}$	6.14	6.43
28.129	5^-	$0d_{3/2}$	$0f_{7/2}$	49.17	52.93
29.855	3^+	$0p_{3/2}$	$0p_{3/2}$	8.65	10.75

TABLE II: The same as in Table I but for the $^{48}_\Lambda\text{K}$ hypernucleus.

of spectra and electroproduction cross sections of $^{40}_\Lambda\text{K}$ and $^{48}_\Lambda\text{K}$ in view of the planned E12-15-008 experiment at JLab.

Our theoretical spectra and cross sections are quite sensitive to the k_F values used for the YN potential, and, therefore, may provide a useful tool for a more detailed study of the properties of both effective YN and modern realistic nuclear potentials.

According to the theoretical analysis of the electroproduction of $^{40}_\Lambda\text{K}$ and $^{48}_\Lambda\text{K}$, important contributions to the cross section should come from the longitudinal mode of the virtual photon suggesting that reliable results can be provided only by the electroproduction calculation.

In order to provide a more complete information in view of the planned E12-15-008 experiment, we intend to include other effective YN and the three-body YNN interactions and to improve the description of the structure by performing our EMPM_Λ calculation within a larger multiphonon space.

ACKNOWLEDGEMENT

The authors thank Jiří Mareš, John Millener, and Petr Navrátil for useful discussions. We thank Petr Navrátil

also for providing us with the matrix elements of the NNLO_{sat} potential. The work was partly supported by the Czech Science Foundation GACR, Grant No. P203-23-06439S. This work is co-funded by EU-FESR, PON Ricerca e Innovazione 2014-2020 - DM 1062/2021. P.V. thanks the INFN for financial support. Computational resources were provided by the CESNET LM2015042 and the CERIT Scientific Cloud LM2015085, under the program “Projects of Large Research, Development, and Innovations Infrastructures”.

-
- [1] A. Gal, E.V. Hungerford, and D.J. Millener, *Rev. Mod. Phys.* **88**, 035004 (2016).
 - [2] *Topics in Strangeness Nuclear Physics*, edited by P. Bydžovský, A. Gal, and J. Mareš, *Lecture Notes in Physics* **724**.
 - [3] O. Hashimoto and H. Tamura, *Prog. Part. Nucl. Phys.* **57**, 564 (2006).
 - [4] *Hypernuclei and Baryon-Baryon Interaction*, edited by E. Hiyama, T. Motoba, and Y. Yamamoto, *Prog. Theor. Phys. Suppl.* **185** (2010).
 - [5] D.J. Millener, *Nucl. Phys. A* **804**, 84 (2008); **835**, 11 (2010); **881**, 298 (2012).
 - [6] O. Benhar, F. Garibaldi, P.E.C. Markowitz, S.N. Nakamura, J. Reinhold, L. Tang, and G.M. Urciuoli (spokespersons), JLab experiment E12-20-013, Studying Λ interactions in nuclear matter with the $^{208}\text{Pb}(e,e'\text{K}^+)^{208}_{\Lambda}\text{Tl}$ reaction, https://www.jlab.org/exp_prog/proposals/20prop.html.
 - [7] F. Garibaldi *et al.*, *Phys. Rev. C* **99**, 054309 (2019).
 - [8] P. Bydžovský, D. Denisova, D. Skoupil, and P. Veselý, *Phys. Rev. C* **106**, 044609 (2022).
 - [9] P. Bydžovský, D.J. Millener, F. Garibaldi, and G.M. Urciuoli, in the 13th Int. Conf. on Hypernuclear and Strange Particle Physics: HYP2018, 24–29 June 2018, Virginia, ed. by L. Tang and R. Schumacher, *AIP Conf. Proc.* **2130**, 020014 (2019).
 - [10] T. Mart, L. Tiator, D. Drechsel, and C. Bennhold, *Nucl. Phys. A* **640**, 235 (1998).
 - [11] T. Mart and B.I.S. van der Ventel, *Phys. Rev. C* **78**, 014004 (2008).
 - [12] We regret having overlooked these two works in Ref. [8]. P. Bydžovský fully assumes responsibility for this omission and apologizes for it.
 - [13] T. Mart, C. Bennhold, H. Haberzettl, and L. Tiator, <http://www.kph.uni-mainz.de/MAID/kaon/>.
 - [14] F. Garibaldi, P.E.C. Markowitz, S.N. Nakamura, J. Reinhold, L. Tang, and G.M. Urciuoli (spokespersons), JLab experiment E12-15-008, An isospin dependence study of the ΛN interaction through the high precision spectroscopy of Λ -hypernuclei with electron beam, https://www.jlab.org/exp_prog/proposals/16/C12-15-008.pdf.
 - [15] S.N. Nakamura, private communication on the upgraded proposal.
 - [16] T. Motoba, M. Sotona and K. Itonaga, *Prog. Theor. Phys. Suppl.* **117**, 123 (1994).
 - [17] M. Sotona and S. Frullani, *Prog. Theor. Phys. Suppl.* **117**, 151 (1994).
 - [18] T. Motoba, P. Bydžovský, M. Sotona, and K. Itonaga, *Prog. of Theor. Phys. Supp.* **185**, 224 (2010).
 - [19] P. Bydžovský, M. Sotona, T. Motoba, K. Itonaga, K. Ogawa, and O. Hashimoto, *Nucl. Phys. A* **881** (2012) 199.
 - [20] T. Motoba, *JSP Conf. Proc.* **17**, 011003 (2017).
 - [21] J. Cohen, *Phys. Rev. C* **32**, 543 (1985).
 - [22] M. Isaka, Y. Yamamoto, and T. Motoba, *Phys. Rev. C* **101**, 024301 (2020).
 - [23] A. Umeyama, T. Motoba, and K. Itonaga, *EPJ Web of Conferences* **271**, 01010 (2022).
 - [24] T. S. H. Lee, Z. Y. Ma, B. Saghai, and H. Toki, *Phys. Rev. C* **58**, 1551 (1998).
 - [25] R. Shyam, H. Lenske, and U. Mosel, *Phys. Rev. C* **77**, 052201(R) (2008).
 - [26] R. Shyam, *Prog. Part. Nucl. Phys.* **61**, 212 (2008).
 - [27] C. Bennhold and L.E. Wright, *Phys. Rev. C* **39**, 927 (1989).
 - [28] C. Bennhold and L.E. Wright, *Phys. Lett. B* **191**, 11 (1987).
 - [29] A. Ekström, G. R. Jansen, K. A. Wendt, G. Hagen, T. Papenbrock, B. D. Carlsson, C. Forssén, M. Hjorth-Jensen, P. Navrátil, and W. Nazarewicz, *Phys. Rev. C* **91**, 051301(R) (2015).
 - [30] P. Veselý, G. De Gregorio, and J. Pokorný, *Phys. Scr.* **94**, 014006 (2019).
 - [31] D. Bianco, F. Knapp, N. Lo Iudice, F. Andreozzi, and A. Porrino, *Phys. Rev. C* **85**, 014313 (2012).
 - [32] G. De Gregorio, F. Knapp, N. Lo Iudice, and P. Veselý, *Phys. Rev. C* **94**, 061301(R) (2016); **95**, 034327 (2017); **97**, 034311 (2018); **99**, 014316 (2019); **101**, 024308 (2020); **105**, 024326 (2022).
 - [33] G. De Gregorio, J. Herko, F. Knapp, N. Lo Iudice, and P. Veselý, *Phys. Rev. C* **95**, 024306 (2017).
 - [34] G. De Gregorio, F. Knapp, N. Lo Iudice, and P. Veselý, *Phys. Scr.* **92**, 074003 (2017).
 - [35] G. De Gregorio, F. Knapp, N. Lo Iudice, and P. Veselý, *Phys. Lett. B* **821**, 136636 (2021).
 - [36] J. Pokorný, G. De Gregorio, F. Knapp, N. Lo Iudice, and P. Veselý, *Act. Phys. Pol. B* **51**, 617 (2020).
 - [37] P. Veselý, G. De Gregorio, F. Knapp, D. Petrellis, P. Bydžovský, D. Denisova, J. Pokorný, D. Skoupil, and N. Lo Iudice, *EPJ Web of Conf.* **271**, 01012 (2022).
 - [38] D. Petrellis, P. Veselý, G. De Gregorio, F. Knapp, P.

- Bydžovský, D. Denisova, J. Pokorný, D. Skoupil, and N. Lo Iudice, J. Phys. Conf. Ser. **2453**, 012009 (2023).
- [39] Y. Yamamoto, T. Motoba, H. Himeno, K. Ikeda, and S. Nagata, Prog. Theor. Phys. Suppl. **117**, 361 (1994).
- [40] D. Skoupil and P. Bydžovský, Phys. Rev. C **97**, 025202 (2018).
- [41] T. Mizutani, C. Fayard, G.-H. Lamot, and B. Saghai, Phys. Rev. C **58**, 75 (1998).
- [42] F. Cusanno et al, Phys. Rev. Lett. **103**, 202501 (2009).
- [43] H. Tamura et al, Nucl. Phys. A **914**, 99 (2013).
- [44] E. Friedman and A. Gal, arXiv:2306.06973[nucl-th].
- [45] B.H. Wildenthal, in: D.H. Wilkinson (Ed.), Progress in Particle and Nuclear Physics, Vol. 11, ed. D.H. Wilkinson (Pergamon, Oxford 1984).